Results in Physics 15 (2019) 102662

Contents lists available at ScienceDirect

Results in Physics

journal homepage: www.elsevier.com/locate/rinp

Color analysis based on the color indices of lightning channels obtained from a digital photograph

Nobuaki Shimoji[a,*], Takahiro Nakano[b]

[a] Faculty of Engineering, University of the Ryukyus, 1 Senbaru, Nishihara, Okinawa 903-0213, Japan
[b] Department of Electrical and Electronics Engineering, University of the Ryukyus, 1 Senbaru, Nishihara, Okinawa 903-0213, Japan

ARTICLE INFO

2010MSC:
00–01
99–00

Keywords:
Lightning photometry
Color index
Color-magnitude diagram
Color-color diagram
2D color index
2D brightness

ABSTRACT

In this study, we present an analysis using the color indices *B-G*, *B-R*, and *G-R* of lightning channels obtained from a digital photograph. We used color-magnitude diagrams (CMDs) modified from the traditional CMDs employed in astronomical photometry, (*B-G*) versus (*G-R*) color-color diagrams (CCDs), two-dimensional (2D) color-index images for the color indices *B-G*, *B-R*, and *G-R*, and a 2D brightness image to analyze the colors and brightness of the lightning channels. The CMDs and CCDs for the lightning leader channels showed that the intensity of B-band and R-band light from those channels exceeds that of the G-band light. The 2D color-index images for *B-G*, *B-R*, and *G-R* and the 2D brightness image indicate spatial variations in the lightning channels. The spatial variabilities of the 2D color indices and 2D brightness indicate that the intensity of the B-band light exceeds that of the G- and R-band light around a bright channel with a high electric current (i.e., the plasma is highly ionized).

Introduction

It is known that a lightning leader channel contains a thermal plasma, that is characterized by high temperature (~30,000 K), high pressure (~10 atm), and electron density (~ 3×10^{24} m^{-3}) [1–8], where these are calculated under local thermodynamic equilibrium. The electric current intensity in a lightning discharge lies in the range of a few hundred kiloamperes. Hariharan et al. recently observed lightning discharges using a muon telescope and reported an electric potential of 1.3 GV [9]. The channel plasma of the lightning emits very bright light. The plasma density, temperature, and energy in the lightning channel increase as the electric current increases (this is known as the Z-pinch effect). The intensity of shorter-wavelength light, the brightness intensity, and the degree of ionization of the plasma increase as its energy increases. Therefore, short-wavelength light is radiated from a high-energy plasma channel that is brighter and exhibits a higher degree of ionization relative to a low-energy plasma channel. Thus, analyzing the color and brightness of a plasma channel exposes its properties in detail.

Several methods for analyzing light exist, including spectroscopy, photometry, and radiometry. So far, spectroscopy is frequently utilized in lightning research. In broad fields like astronomy, illumination engineering, and color science, spectroscopy and photometry are utilized in combination. Many observations in astronomy were independently developed, and have long history.

In astronomy, the analysis of light radiated from stars is based on astronomical photometry. Stellar observations relied on the naked eye from the 2nd century BC to the middle of the 19th century. The use of photography in astronomy began in the middle of the 19th century. Currently, charge-coupled device/complementary metal-oxide semiconductor (widely known as CCD/CMOS) image-sensor devices are being used in astronomy (for a brief history of astronomy, see, e.g., Section 2.2 in Ref. [10]). The surface temperatures of stars are evaluated by observing their colors and brightness, since the surface of a star is similar to a Planckian radiator (for astronomical photometry, see, e.g., Ref. [10]). The color index and magnitude of a star are related to its actual temperature and energy density, respectively. For a lightning leader channel, from the Z-pinch effect the short-wavelength light and brightness intensity increase as the electric current in the lightning leader channel increases. That is, the color and brightness of a lightning leader channel are related to its energy, ionization, and current. Therefore, photometry using the color index and magnitude system developed in astronomy also can be applied to lightning research.

Lightning flashes are a natural source of light. In general, the light from a light source is often analyzed by spectroscopy, photometry or radiometry in many fields. In illumination engineering and color science, the color of a light source is evaluated using several color spaces, including RGB and XYZ color spaces (for color spaces, see, e.g., Chapter

* Corresponding author.
E-mail address: nshimoji@tec.u-ryukyu.ac.jp (N. Shimoji).

https://doi.org/10.1016/j.rinp.2019.102662
Received 12 July 2019; Received in revised form 19 August 2019; Accepted 12 September 2019
Available online 23 September 2019

12 in Ref. [11]).

In a previous study [12], we reported a correlated color temperature (CCT) of lightning channels in a digital photograph. We also reported a brightness evaluation of those lightning channels by utilizing the magnitude system employed in astronomical photometry [13,14]. Research using color analyses and brightness evaluations of lightning are part of lightning photometry. The aim of this study, therefore, is to advance lightning photometry.

Recently, with the development of measuring devices, there has been an increase in interesting studies of lightning using high-speed video cameras (see, e.g., [15–23]). These studies were mostly recorded using a digital still camera or digital movie camera. Lightning photometry will therefore be applicable to the analysis of lightning discharges in the future, although lightning photometry is a new method that is still developing.

In this study, to perform lightning photometry, we constructed color-magnitude diagrams (CMDs), color-color diagrams (CCDs), two-dimensional (2D) color-index images for the color indices *B-G*, *B-R*, and *G-R*, and a 2D grayscale image. The CMD used in this study was slightly modified for lightning photometry from the traditional CMD of astronomical photometry. The CMD demonstrated a relationship between the brightness and the color indices of a lightning leader channel, and the CCD showed the color bias of the lightning leader channel. The 2D color-index images showed the colors and spatial information simultaneously. The 2D grayscale image contains the brightness and spatial information about the lightning leader channel, and shows them simultaneously. The CMD, CCD, 2D color-index images, and 2D grayscale image can provide the color, brightness, and 2D spatial variability of the lightning leader channels simultaneously.

Materials and methods

Digital photograph showing a lightning flash

Fig. 1(a) is a photograph exhibiting the lightning flash that was used in this study. This photograph was obtained from a location with coordinates 36.284516°N (latitude), and 139.9638°E (longitude), according to the World Geodetic System 1984. A digital still camera, Canon EOS KISS Digital X, with the lens TAMRON AF28–300 mm F/3.5–6.3 XR Di LD Aspherical [IF] MACRO (Model A061), was used to obtain the photograph. The RGB color filter of the digital camera used in this study is the primary color filter (color-filter characteristics for commercially available digital still camera are summarized in Appendix A.) Photographic filters, such as neutral-density filters or graduated filters, were not used in the capture of Fig. 1(a), and the image data were saved in RAW format (personal communication, Photographer Mr. Yutaka Aoki). Since the RAW data represent unprocessed photo-signals, we developed the image data using the developing software SILKYPIX Developer Studio Pro 7 (Ichikawa Soft Laboratory Co., Ltd., Chiba, Japan), generating an uncompressed TIFF image (see Fig. 1(a)). The properties of the developed digital photograph (Fig. 1(a)) include an image size of 3, 000 × 2, 000 pixels; an sRGB color space; date October 27, 2008, with a start time of 21:31:33 (Japan Standard Time, JST); and an exposure duration of 36 s. (Note that JST is UTC (Coordinated Universal Time) + 9 h.)

The tortuous lightning channels in Fig. 1(a) comprise the left-side and right-side strike channels and many branch-leader channels. In a previous study [13], we determined the currents in the left-side and right-side strike channels to be I_{left} = 11 kA and I_{right} = 35 kA, respectively.

In order to analyze only the lightning leader channels in Fig. 1(a), we extracted the leader channels (see Fig. 1(b)) by applying image-processing techniques (Fig. 2). For the image processing used in this study, we adopted the Open Source Computer Vision Library (known as OpenCV library) version 3.0 [25].

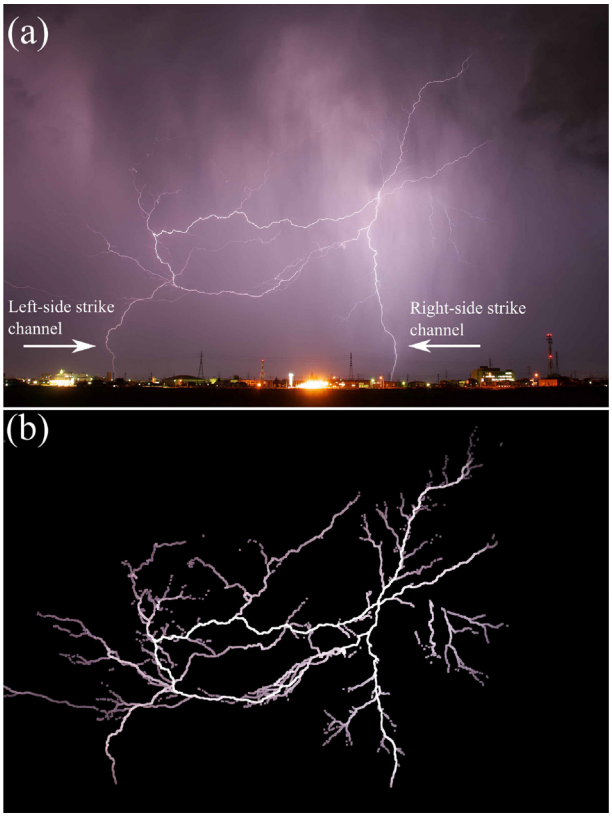

Fig. 1. (a) A digital photograph showing a lightning flash (photo courtesy of Mr. Yutaka Aoki) and (b) lightning channel extracted by image processing. This digital photograph was captured in the city of Chikusei, Ibaraki Prefecture, Japan, on October 27, 2008. The extracted lightning channels were thickened through image processing to improve visibility, since the original channels were thin and barely visible (modified from Ref. [12–14]).

Evaluation of color and brightness

We evaluated the color and brightness of the lightning leader channel (Fig. 1) using CMD, CCD, 2D color-index images, and 2D brightness images. According to the Z-pinch effect, the plasma density and temperature increase with increasing electric current. An increase in plasma temperature causes an increase in the number of excited atoms, enhancing the brightness of the plasma channel. Therefore, a high-brightness leader channel can be considered to have a higher electric current, higher density, higher temperature, and higher number density of excited atoms than a faint leader channel.

In general, a primary RGB color filter is often used in commercially available digital still cameras, and it contains B-, G-, and R-band filters. The band ranges are ~ 400–500 nm for the B-band, ~ 500–600 nm for the G-band, and ~ 600–700 nm for the R-band (see Appendix A). By comparing the B-, G-, and R-channel images, we can obtain the differences in the brightness of a leader channel as seen through the B-, G-, and R-band filters. The differences of the color for the lightning leader channel will exibit the differences of the excited states in the channel plasma. To evaluate the color of the lightning leader channel (Fig. 1), we adopted the color indices *B–G*, *B–R*, and *G–R*.

Apparent magnitude

In order to calculate the apparent magnitude of the lightning channels, we assumed the maximum brightness (maximum pixel value 255 in 256 levels) in each (monochromatic) R, G, and B channel image to be the reference brightness, V_{ref} = 255. Thus, the magnitude of a pixel with the maximum pixel value 255 is zero (i.e., m_{ref} = 0). The apparent magnitude of the *i*th pixel is then given by

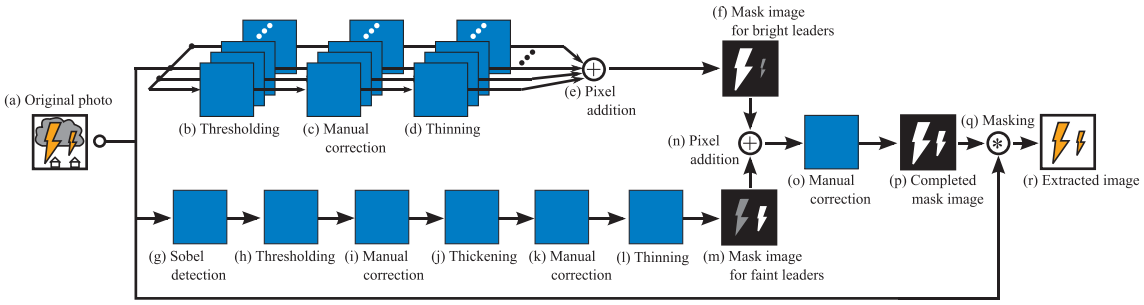

Fig. 2. Flowchart for extracting the lightning leader channels (Fig. 1(b)) from the digital photograph (Fig. 1(a)). The extraction method is based on simple masking; however, many processes (b)–(o) are needed to create the mask image showing the tortuous leader channels. In the thinning processes (d) and (l), we adopted the Zhang-Suen thinning algorithm [24]. The extraction method was slightly modified from that explained in Appendix C of Ref. [13].

$$m_i = -2.5\log_{10}\frac{V_i}{V_{\mathrm{ref}}}, \tag{1}$$

where V_i and V_{ref} are the pixel values for the ith pixel and the reference brightness, respectively [13].

Color indices B-G, B-R, and G-R

We utilized the color indices for astronomical photometry to calculate the colors of the lightning channels in Fig. 1(b). In this study, the color index is defined as

$$X - Y = m_X - m_Y = -2.5\log_{10}\frac{V_X}{V_Y}, \tag{2}$$

where X and Y represent colors like the B, G, and R filters, X–Y indicates the color index between the X- and Y-band filters, m_X and m_Y are the magnitudes of the X- and Y-bands, respectively, and V_X and V_Y are the pixel values for the (monochromatic) X and Y channel images, respectively. It should be noticed that X-$Y < 0$ if X is greater than Y, X-$Y > 0$ if Y is greater than X, and X-$Y = 0$ if X is equal to Y.

CMD

We have constructed CMDs for the lightning channels in Fig. 1(b) using the color indices B-G, B-R, and G-R. We slightly modified the traditional CMD used in astronomical photometry, since the RGB system we use differs from astronomical photometric systems like the Johnson-Cousins UBVRI system. The absolute magnitude or apparent magnitude is used for the vertical axis of the CMD in astronomy. In this study, we substituted the brightness V_{GS} (i.e., the grayscale value) for the absolute or apparent magnitude, whereas we used the color indices B-G, B-R, and G-R for the horizontal axes, as in the traditional CMD in astronomical photometry. The brightness (i.e., the vertical axis) reflects the plasma density, temperature, and ionization of the lightning leader channel, and the color (i.e., the horizontal axis) suggests the excited states or the plasma energy of the lightning leader channel. We denote the modified CMDs used in this study as (V_{GS}, B-G), (V_{GS}, B-R) and (V_{GS}, G-R) (hereinafter referred to as the modified CMDs.)

We assessed the difference between the electric currents $I_{\mathrm{left}} = 11$ kA of the left-side strike channel and $I_{\mathrm{right}} = 35$ kA of the right-side strike channel by constructing CMDs for all the leader channels, the left-side strike channel, and the right-side strike channel.

CCD

We constructed a (B–G) versus (G–R) CCD for all leader channels to analyze the colors of the leader channels in Fig. 1(b), with the color indices B-G and G-R were used as the vertical axis and horizontal axis, respectively. The (B-G) versus (G-R) CCD displays the distribution of the B-G and G-R simultaneously. The result of the CCD suggests the excited states in plasma of the lightning leader channel. The difference in the electric current for the left-side and right-side strike channels ($I_{\mathrm{left}} = 11$ kA and $I_{\mathrm{right}} = 35$ kA) was evaluated by constructing the (B-G) versus (G-R) CCDs for the left-side and right-side strike channels.

2D color-index image

In addition to the modified CMD and CCD, we also obtained 2D color-index images for the color indices B-G, B-R, and G-R (hereinafter denoted $(B–G)_{2D}$, $(B–R)_{2D}$, and $(G–R)_{2D}$). Although the modified CMD contains color and brightness information, it lacks 2D spatial information. The 2D color-index images are actual 2D images of the lightning channels depicted using the color indices B-G, B-R, and G-R. Therefore, the 2D color-index images contain color and 2D spatial information, but not brightness information. In contrast the grayscale image contains brightness and 2D spatial information but lacks color information. Thus, in order to study the color, brightness, and 2D spatial information concurrently, we constructed 2D color-index images with the 2D brightness (grayscale) image. The 2D color-index images and 2D brightness image suggest the excited states of the plasma (i.e., the plasma energy), plasma density, temperature, degree of ionization, and 2D spatial variability simultaneously.

Results and discussion

Modified CMD and CCD

Fig. 3 shows the modified CMDs that is (V_{GS}, B-G), (V_{GS}, B-R), and (V_{GS}, G-R) for the extracted lightning channels in Fig. 1(b). The (V_{GS}, B-G) CMDs (Fig. 3 indicate that the B-band light is brighter than the G-band light (i.e., $B–G < 0$). The (V_{GS}, B-R) CMDs in Fig. 3 show light with B-$R < 0$, B-$R \simeq 0$, and B-$R > 0$. Clearly, in Fig. 3(b) for all leader channels and Fig. 3(e) for the left-side strike channel, the R-band light is brighter than the B-band light (i.e., B-$R \geqslant 0$). However, in Fig. 3(h) for the right-side strike channel, the B-band light is brighter than the R-band light (i.e., B-$R < 0$). In the (V_{GS}, G-R) CMDs in Fig. 3(c), (f), and (i), the R-band light is brighter than the G-band light (i.e., G-$R > 0$).

For the faint-leader (lower-brightness V_{GS}) channels, evidently B-$G < 0$ (see Fig. 3; B-$R > 0$ (Fig. 3(b) and (e)); and G-$R > 0$ (Fig. 3. The right-side strike channel (Fig. 3(h)) exhibits B-$R < 0$ independent of the brightness of the channel. In contrast, for the bright-leader (higher-brightness V_{GS}) channel, the color indices B-G, B-R, and G-R in Fig. 3 converge to zero. In other words, in a faint-leader channel, the intensities of the B-band light and R-band light are stronger than that of the G-band light, whereas in a bright-leader channel, the intensities of the three colors (B-, G- and R-bands) light approaches each other. The increase in the intensity of light emitted from a plasma with increasing energy is well known in plasma physics. Thus, the intensities of the three colors (B-, G- and R-bands) of light likely increase and converge with increasing energy of the plasma of the lightning channel. Also, the intensity of the G-band light probably decreases drastically with decreasing energy of the plasma in the lightning channel.

Fig. 4(a)–(c) show the (B-G) versus (G-R) CCDs for all leader channels as well as for the left-side and right-side strike channels. Fig. 4(a) clearly demonstrates that the intensity of the G-band light is

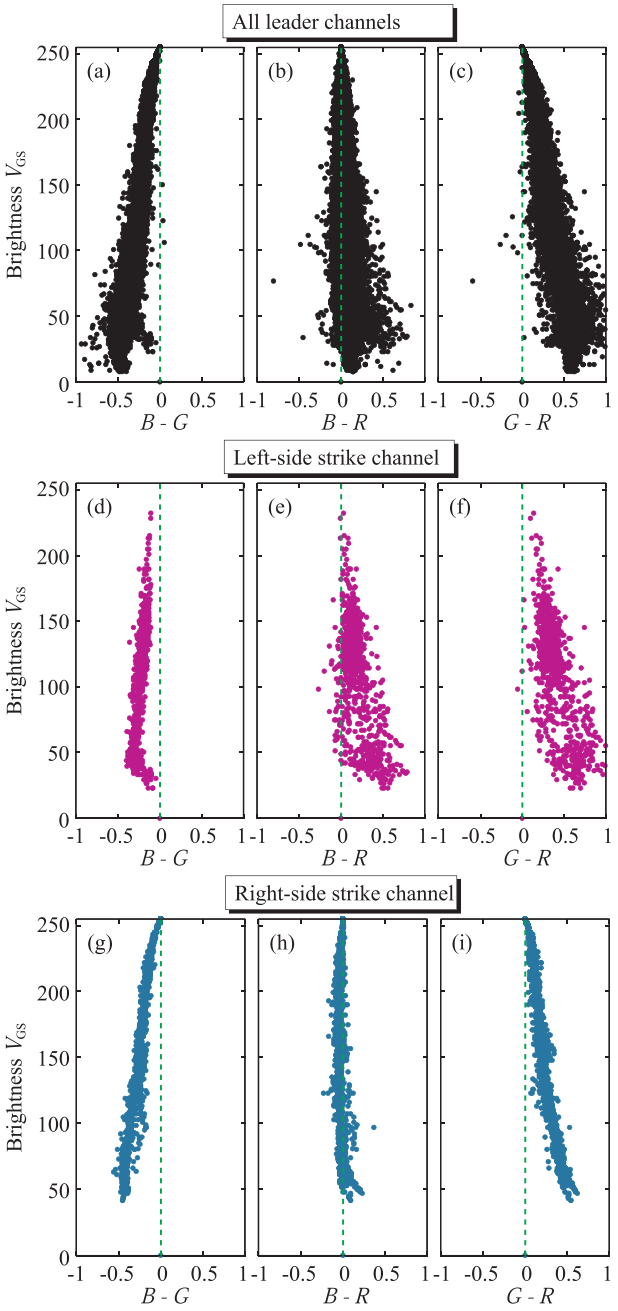

Fig. 3. Modified CMDs (V_{GS}, B-G), (V_{GS}, B-R), and (V_{GS}, G-R) for the extracted lightning channels shown in Fig. 1(b). The top three panels ((a), (b), and (c) colored black) correspond to all the leader channels in Fig. 1(b), the middle three panels ((d), (e), and (f) colored magenta) are the left-side strike channel in Fig. 1(b), and the bottom three panels ((g), (h), and (i) colored dark-cyan) are the right-side strike channel in Fig. 1(b). The vertical broken line (colored green) in each panel indicates the center of each color index B-G = 0, B-R = 0, and G-R = 0. The top three panels ((a), (b), and (c)) were modified from Ref. [14]. (For interpretation of the references to colour in this figure legend, the reader is referred to the web version of this article.)

lower than that of the B- and R-bands. Fig. 4(b) indicates that for the left-side strike channel the intensity of the R-band light is greater than that of the B-band light. Conversely, Fig. 4(c) shows that for the right-side strike channel the intensity of the B-band light is greater than that of the R-band light. These results from the CCDs (Fig. 4) are consistent with the results from the CMDs in Fig. 3.

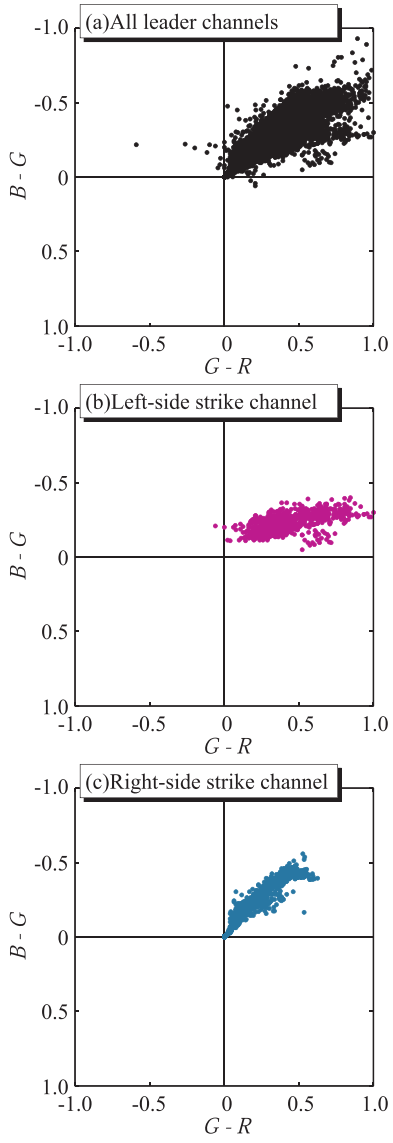

Fig. 4. (B-G) versus (G-R) CCDs for (a) all leader channels (colored black), (b) the left-side strike channel (colored magenta), and (c) the right-side strike channel (colored dark-cyan), shown in Fig. 1(b). (For interpretation of the references to colour in this figure legend, the reader is referred to the web version of this article.)

2D color-index and 2D brightness of the lightning channels

From Fig. 3(h), the right-side strike channel exhibits light with the colors B-$R < 0$, B-$R \simeq 0$, and B-$R > 0$. However, the spatial variability of the color index remains unknown, because the modified CMD and CCD lack 2D spatial information. Consequently, we created 2D color-index images $(B\text{-}G)_{2D}$, $(B\text{-}R)_{2D}$, and $(G\text{-}R)_{2D}$ and a 2D brightness (grayscale) image for the extracted lightning channels in Fig. 1(b). Fig. 5 shows the 2D color-index images $(B\text{-}G)_{2D}$, $(B\text{-}R)_{2D}$, and $(G\text{-}R)_{2D}$ and the 2D brightness (grayscale) image for the extracted channel (Fig. 1(b)). The intensities of the B-band light and R-band light are greater than that of the G-band light (Fig. 5(a) and (c)). Fig. 5(b) also demonstrates that the B-band light is brighter than the R-band light around part of the right-side strike channel (see also Fig. 6); however, the R-band light is brighter than the B-band light around the left-side strike channel and the other branch channels. Short-wavelength light occurs mainly around the right-side strike channel, with a brighter right-side strike channel relative to the left-side strike channel (Fig. 5(d)), which is explained in Ref. [13] using the magnitude system.

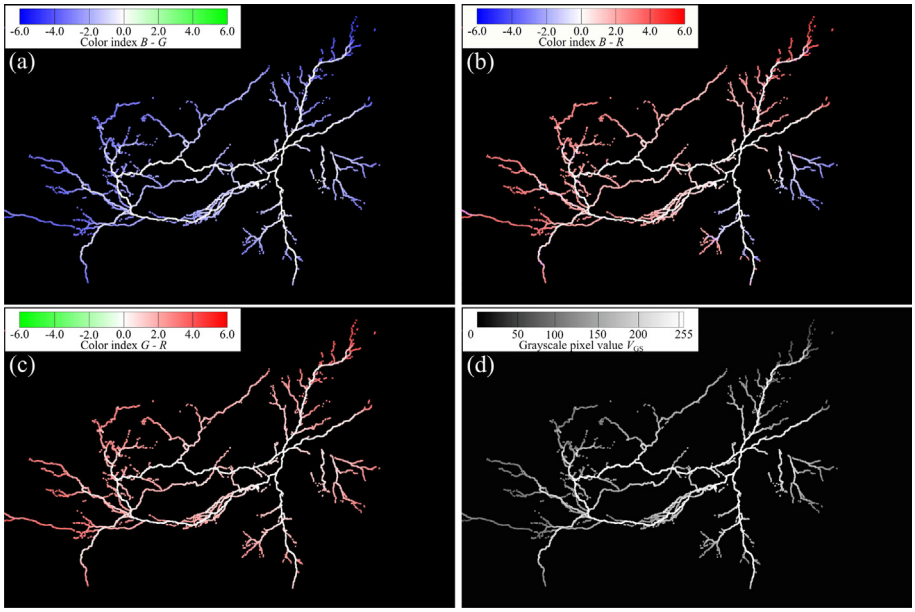

Fig. 5. 2D color-index images of (a) $(B\text{-}G)_{2D}$, (b) $(B\text{-}R)_{2D}$, and (c) $(G\text{-}R)_{2D}$ and (d) grayscale image for the extracted lightning channel in Fig. 1(b). The scale bars in (a), (b) and (c) denote the color indices *B-G*, *B-R*, and *G-R*, respectively, whereas the scale bar in (d) denotes the brightness (grayscale pixel value) V_{GS} (in 256 levels). We thickened the lightning channels by applying image processing to improve visibility, since they were very thin and thus less visible (modified from Ref. [14]). (For interpretation of the references to colour in this figure legend, the reader is referred to the web version of this article.)

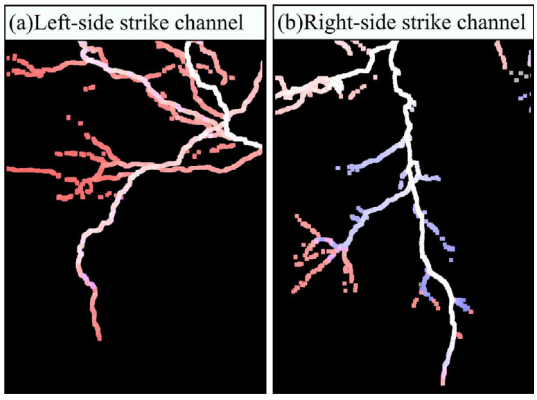

Fig. 6. Enlarged images of (a) the left-side strike channel and (b) the right-side strike channel in Fig. 5(b). The left-side strike channel has $B\text{-}R > 0$ (reddish), while the right-side strike channel largely has $B\text{-}R < 0$ (bluish). However, a few segments with $B\text{-}R > 0$ (reddish) exist on the right-hand side. (For interpretation of the references to colour in this figure legend, the reader is referred to the web version of this article.)

A plasma emits bright light when it possesses higher energy (i.e., high density and highly ionized). Hence, we infer that the right-side strike channel contains higher energy and emits shorter-wavelength light compared to the left-side strike channel. Simply put, the highly ionized bright channel emits shorter-wavelength light. As explained in a previous study [13], the channel currents of the left- and right-side strike channels in Fig. 1 are 11 kA and 35 kA, respectively (i.e., $I_{left} < I_{right}$). Thus, the spatial variability of the B-, G-, and R-bands of the lightning channels is related to the channel current and channel energy. The results described here may be related to the relation between channel CCT and channel current reported in Ref. [12]. In that work we reported that the CCT of the right-side strike channel is greater than that of the left-side strike channel: $T_{left}^{CCT} < T_{right}^{CCT}$. It has also been reported that there is a correlation between channel brightness and channel current [26–31]. From the above, the brightness and CCT of the lightning leader channel increase, and the color index *B–R* increases negatively, with increasing electric current in the lightning leader channel.

In this study, we focused on the colors, brightness, and spatial variability of the lightning channels. The lightning photometry reported in this study and in previous studies [12–14] may influence the diagnosis of lightning channels.

Conclusions

In this study, we calculated the color indices *B-G*, *B-R*, and *G-R* of the lightning channels shown in a digital photograph (Fig. 1(b)). The modified CMDs (V_{GS}, *B-G*), (V_{GS}, *B-R*), and (V_{GS}, *G-R*) and the (*B-G*) versus (*G-R*) CCD confirm that for all leader channels and for the leftl-side strike channel the colors are $B\text{-}G < 0$ and $G\text{-}R > 0$, and for the right-side strike channel, the color is $B\text{-}R < 0$, but there was also a slight amount of $B\text{-}R \geqslant 0$. In particular, the color indices *B-G*, *B-R*, and *G-R* converged to zero at the bright channel. At the faint channel, the intensity of the G-band light decreased drastically. The 2D color-index images $(B\text{-}G)_{2D}$, $(B\text{-}R)_{2D}$, and $(G\text{-}R)_{2D}$ and the 2D grayscale image for the lightning channels confirmed the spatial variabilities of the color indices *B-G*, *B-R*, and *G-R* and brightness. It is noteworthy that, in the 2D color-index image $(B\text{-}R)_{2D}$, the B-band light is brighter than that of the R-band around the brighter channel (i.e., the right-side strike channel). The results for the modified CMD, the CCD, and the 2D color-index images suggest that the color index is useful for the evaluation of lightning channels.

Declaration of Competing Interest

The authors declare that they have no known competing financial interests or personal relationships that could have appeared to influence the work reported in this paper.

Acknowledgements

We would like to thank Mr. Yutaka Aoki, a freelance photographer specializing in storms, for providing the digital photograph (RAW data) showing the lightning flash. We are also grateful to Mr. Wataru Hasegawa, Mr. Yamato Uehara, Mr. Shouta Kuninaka, Ms. Kana Izumi, and Mr. Keito Tamaki for their valuable discussions and assistance with

Table 1
Peak wavelengths and FWHMs of the primary RGB color filter (adapted from Fig.5.34 in Ref. [33]) and of the UBVRI color filters [32]. The data for the UBVRI filter curves were downloaded from the website of the Leibniz-Institut für Astrophysik Potsdam (http://www.aip.de/en/research/facilities/stella/instruments/data), (last accessed on October 26, 2016).

Filter	Peak wavelength/ nm			FWHM/ nm			Source
	B	G	R	B	G	R	
RGB	~ 448	~ 527	~ 614	~ 100	~ 98	~ 130	Fig. 5.34 in Ref. [33]
	B	V	R	B	V	R	
UBVRI	421.5	521.5	595	78.1	99.1	106.56	Ref. [32]

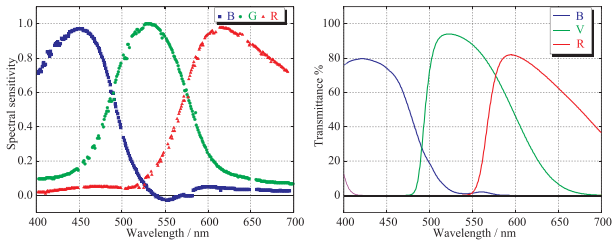

Fig. 7. (a) RGB filter curves of a primary color filter (adapted from Ref. [33]) and (b) Johnson-Cousins UBVRI filter curves [32] (downloaded from the website of the Leibniz-Institut für Astrophysik Potsdam:http://www.aip.de/en/research/facilities/stella/instruments/data, last accessed on October 26, 2016). The filter curves are shown in the wavelength range 4.00 nm–700 nm.

the image processing, as well as Dr. Akira Yonesu, a Professor at the Faculty of Engineering, University of the Ryukyus, for the valuable discussion on plasma physics. The authors are grateful to anonymous reviewers for useful comments. The authors would also like to thank Enago (www.enago.jp) for the English language review. This research was not supported by any funding agencies in the public, commercial, or not-for-profit sectors.

Color-filter characteristics

The color-filter characteristics of the primary RGB color filter are shown in Table 1 and Fig. 7. While the FWHM of the R-band filter is greater than 100 nm, it will become ~ 100 nm with an IR-cut filter. For reference, the filter characteristics of the Johnson-Cousins UBVRI filters [32] often used in astronomical photometry are shown in Table 1 and Fig. 7.

References

[1] Uman MA, Orville RE. Electron density measurement in lightning from stark-broadening of H α. J Geophys Res 1964;69:5151–4. https://doi.org/10.1029/JZ069i024p05151.
[2] Uman MA, Orville RE, Salanave LE. The mass density, pressure, and electron density in three lightning strokes near peak temperature. J Geophys Res 1964;69:5423–4. https://doi.org/10.1029/JZ069i024p05423.
[3] Uman MA, Orville RE, Salanave LE. The density, pressure, and particle distribution in a lightning stroke near peak temperature. J Atmospheric Sci 1964;21:306–10. https://doi.org/10.1175/1520-0469(1964) 021<0306:TDPAPD>2.0.CO;2.
[4] Uman MA, Orville RE. The opacity of lightning. J Geophys Res 1965;70:5491–7. https://doi.org/10.1029/JZ070i022p05491.
[5] Orville RE. Spectrum of the lightning stepped leader. J Geophys Res 1968;73:6999–7008. https://doi.org/10.1029/JB073i022p06999.
[6] Orville RE. A high-speed time-resolved spectroscopic study of the lightning return stroke: Part i. a qualitative analysis. J Atmospheric Sci 1968;25:827–38. https://doi.org/10.1175/1520-0469(1968)025<0827:AHSTRS>2.0.CO;2.
[7] Orville RE. A high-speed time-resolved spectroscopic study of the lightning return stroke: Part ii. a quantitative analysis. J Atmospheric Sci 1968;25:839–51. https://doi.org/10.1175/1520-0469(1968) 025<0839:AHSTRS>2.0.CO;2.
[8] Orville RE. A high-speed time-resolved spectroscopic study of the lightning return stroke. part iii. a time-dependent model. J Atmospheric Sci 1968;25:852–6. https://doi.org/10.1175/1520-0469(1968)025<0852:AHSTRS>2.0.CO;2.
[9] Hariharan B, Chandra A, Dugad SR, Gupta SK, Jagadeesan P, Jain A, Mohanty PK, Morris SD, Nayak PK, Rakshe PS, Ramesh K, Rao BS, Reddy LV, Zuberi M, Hayashi Y, Kawakami S, Ahmad S, Kojima H, Oshima A, Shibata S, Muraki Y, Tanaka K. Measurement of the electrical properties of a thundercloud through muon imaging by the grapes-3 experiment. Phys Rev Lett 2019;122. https://doi.org/10.1103/PhysRevLett. 122.105101. 105101.
[10] Budding E, Demircan O. Introduction to Astronomical Photometry. 2nd Edition New York, USA: Cambridge University Press; 2007.
[11] Burger W, Burge MJ. Digital Image Processing: An Algorithmic Introduction using Java. 1st Edition LLC, New York, USA: Springer Science+Business Media; 2008.
[12] Shimoji N, Aoyama R, Hasegawa W. Spatial variability of correlated color temperature of lightning channels. Results Phys 2016;6:161–2. https://doi.org/10.1016/j.rinp.2016.03.004.
[13] Shimoji N, Kuninaka S, Izumi K. Evaluation of the brightness of lightning channels and branches using the magnitude system: Application of astronomical photometry. Results Phys 2017;7:2085–95. https://doi.org/10.1016/j.rinp.2017.06.013.
[14] Shimoji N, Uehara Y. Color analysis of lightning leaders: Application of astronomical photometry. AIP Conf Proc 2017;1906. https://doi.org/10.1063/1.5012310. 030030.
[15] Zhang Y, Lu W, Li J, Dong W, Zheng D, Chen S. Luminosity characteristics of leaders in natural cloud-to-ground lightning flashes. Atmos Res 2009;91:326–32. https://doi.org/10.1016/j.atmosres.2008.01.013.
[16] Mazur V, Ruhnke LH. Physical processes during development of upward leaders from tall structures. J Electrostat 2011;69:97–110. https://doi.org/10.1016/j.elstat.2011.01.003.
[17] Warner TA. Observations of simultaneous upward lightning leaders from multiple tall structures. Atmos Res 2012;117:45–54. https://doi.org/10.1016/j.atmosres.2011.07.004.
[18] Montanyà J, van der Velde OA, March V, Romero D, Solà G, Pineda N. High-speed video of lightning and x-ray pulses during the 2009–2010 observation campaigns in northeastern spain. Atmos Res 2012;117:91–8. https://doi.org/10.1016/j.atmosres.2011.09.013.
[19] Mazur V, Ruhnke LH, Warner TA, Orville RE. Recoil leader formation and development. J Electrostat 2013;71:763–8. https://doi.org/10.1016/j.elstat.2013.05.001.
[20] Campos LZ, Saba MM, Warner TA, Pinto Jr. O, Krider EP, Orville RE. High-speed video observations of natural cloud-to-ground lightning leaders - a statistical analysis. Atmos. Res. 2014;135–136:285–305. https://doi.org/10.1016/j.atmosres.2012.12.011.
[21] Saba MM, Schumann C, Warner TA, Helsdon JH, Orville RE. High-speed video and electric field observation of a negative upward leader connecting a downward positive leader in a positive cloud-to-ground flash. Electr Pow Syst Res 2015;118:89–92. https://doi.org/10.1016/j.epsr.2014.06.002.
[22] Mazur V. The physical concept of recoil leader formation. J Electrostat 2016;82:79–87. https://doi.org/10.1016/j.elstat.2016.05.005.
[23] Mazur V. On the nature of bipolar flashes that share the same channel to ground. J Electrostat 2017;90:31–7. https://doi.org/10.1016/j.elstat.2017.09.002.
[24] Zhang TY, Suen CY. A fast parallel algorithm for thinning digital patterns. Commun ACM 1984;27:236–9. https://doi.org/10.1145/357994.358023.

[25] Bradski G, Kaehler A. Learning OpenCV: Computer vision with the OpenCV library. 1st Edition USA: O'Reilly Media Inc; 2008.
[26] Flowers JW. The channel of the spark discharge. Phys Rev 1943;64:225–35. https://doi.org/10.1103/PhysRev. 64.225.
[27] Idone VP, Orville RE. Correlated peak relative light intensity and peak current in triggered lightning subsequent return strokes. J Geophys Res Atmos 1985;90:6159–64. https://doi.org/10.1029/JD090iD04p06159.
[28] Gomes C, Cooray V. Correlation between the optical signatures and current wave forms of long sparks: applications in lightning research. J Electrostat 1998;43:267–74. https://doi.org/10.1016/S0304-3886(98)00008-4.
[29] Wang D, Takagi N, Watanabe T, Rakov VA, Uman MA, Rambo KJ, Stapleton MV. A comparison of channel-base currents and optical signals for rocket-triggered lightning strokes. Atmos Res 2005;76:412–22. https://doi.org/10.1016/j.atmosres.2004.11.025.
[30] Amarasinghe D, Sonnadara U, Berg M, Cooray V. Correlation between brightness and channel currents of electrical discharges. IEEE Trans Dielect Electr Insul 2007;14:1154–60. https://doi.org/10.1109/TDEI.2007.4339475.
[31] Zhou E, Lu W, Zhang Y, Zhu B, Zheng D, Zhang Y. Correlation analysis between the channel current and luminosity of initial continuous and continuing current processes in an artificially triggered lightning flash. Atmos Res 2013;129–130:79–89. https://doi.org/10.1016/j.atmosres.2012.10.020.
[32] Strassmeier KG, Granzer T, Weber M, Woche M, Andersen MI, Bartus J, Bauer S-M, Dionies F, Popow E, Fechner T, Hildebrandt G, Washuettl A, Ritter A, Schwope A, Staude A, Paschke J, Stolz PA, Serre-Ricart M, de la Rosa T, Arnay R. The STELLA robotic observatory. Astron Nachr 2004;325:527–32. https://doi.org/10.1002/asna.200410273.
[33] Yonemoto K. Foundations and applications of CCD/CMOS image sensor [CCD/CMOS image sensor no kiso to ouyou]. CQ Publishing; 2003. (in Japanese).